Journal of Membrane Science 551 (2018) 223–233

Contents lists available at ScienceDirect

Journal of Membrane Science

journal homepage: www.elsevier.com/locate/memsci

Modeling of cross flow hollow fiber ultrafiltration for treatment of effluent from Railway Workshop

Krishnasri V. Kurada, Tanmay, Sirshendu De*

Department of Chemical Engineering, Indian Institute of Technology Kharagpur, Kharagpur 721302, India

ARTICLE INFO

Keywords:
Oil
Ultrafiltration
Hollow fiber
Cake filtration
Permeate flux

ABSTRACT

Industrial oily water containing oil, grease and dust has been treated using stage-wise filtration, first by sand bed followed by cross-flow ultrafiltration hollow fiber membrane. The sand bed removes majority of suspended particles and reduces the turbidity from 13.6 NTU to 2.6 NTU. Effects of transmembrane pressure drop and cross flow rate on ultrafiltration performance were investigated. A transport phenomena based model under the framework of boundary layer theory was developed to quantify the flux decline and oil transport through the membrane during cross flow filtration in hollow fiber. The model results matched remarkably well with the experimental data. The mechanism of filtration was analyzed and found to be governed by cake formation. Formation of cake-layer was supported by scanning electron micrography of fresh and fouled membranes and Fourier Transform Infrared spectroscopy. The modeling of separation mechanism and estimates system parameters will aid in scaling up of the filtration set-up to industrial scale for treatment of industrial effluent containing oil.

1. Introduction

Oil and grease are integrated components of many industrial effluent streams. Nature of the oily contaminant varies widely from vegetable oils to hydrocarbons and mineral oils depending on the source. Typical concentration of oil in effluent from petroleum industry varies between 10 and 3200 mg/l, whereas, the same in case of steel and aluminum industries range between 5000 and 50000 mg/l [1,2]. Car production effluent contains even higher oil and grease in the range 200 g/l [3]. Oil in such effluent includes hydrocarbons which, even in trace quantities, may harm the marine life. Oil-in-water emulsions in industrial effluent are generated from equipment wash water, rinsing baths, compressor condensates, etc., and considerable amount of such oily effluent cannot be treated using biochemical degradation [4]. The maximum permissible limit of oil in discharge stream is categorized based on the source and nature of contaminant. To cite a few, according to the US regulations, the limit of oil in effluent stream from petroleum refinery is limited to 5 mg/l [5], whereas, the same for hardware industries is 35 mg/l for one day and cannot exceed 17 mg/l over a period of month [1]. Existing Indian standard for discharge of oily water to surface is 10 mg/l oil concentration and is proposed to be reduced further to 5 mg/l [6]. This makes the removal of oil more crucial even in traces.

Treatment of oil from waste water can be divided broadly into two categories, namely, primary treatment and secondary treatment [2]. Primary treatment aims at removing floating oil and to some extent emulsified oil, whereas, secondary treatment is used to remove oil present in low concentration. Several conventional techniques are employed for removal of oil and grease from waste water streams including gravity settling, API separator, centrifugal settling, de-emulsification using chemical agents, electrostatic coalescence, skimming, air floatation, flocculation etc. [1,7–9]. Each of these conventional techniques possesses advantages and disadvantages of its own. Gravity settling, API separator, skimming, etc., are effective in removing larger droplets and emulsions but result very low efficiency for smaller droplets. Flotation and coagulation (both chemical and electrostatic) methods typically employ chemical agents generating large amount of sludge [1,10]. The major drawback of these conventional techniques is that their efficiency falls when the droplet size in emulsion is below 10 μm and concentration is less than 1% by volume [2,5].

In case, where effluent stream is a dilute solution containing micron range particles, membranes are attractive alternative. Applicability of membranes in removal of oil-water emulsions is increasing rapidly due to stable filtrate quality and small area requirement [10]. Also membrane based processes do not require external chemicals and hence, generate negligible amount of sludge. Cheryan et al., have provided significant review of various methods being followed for removal of oil from water with the help of polymeric membranes [1]. According to

* Corresponding author.
E-mail address: sde@che.iitkgp.ernet.in (S. De).

https://doi.org/10.1016/j.memsci.2018.01.051
Received 30 November 2017; Received in revised form 19 January 2018; Accepted 20 January 2018

Nomenclature

a and b	Pressure dependence parameters of mass transfer coefficient, unit of b [Pa^{-1}]
B	Solute permeability through the membrane [kg/(m^2 s)]
c	Oil concentration [mg/l]
c_{avg}	Average solute concentration in the membrane phase [mg/l]
c_c	Oil concentration in cake layer [mg/l]
CFR	Cross flow rate [l/h]
c_p	Oil concentration in permeate [mg/l]
c_p^s	Oil concentration in permeate at steady state [mg/l]
c_0	Oil concentration in feed [mg/l]
D	Diffusivity of oil in water [m^2/s]
d	Hollow fiber inner diameter [μm]
J	Permeate flux at any time point [l/(m^2 h)]
J^s	Permeate flux at steady state l/(m^2 h)]
$J^{s,cal}$	Steady state permeate flux: calculated values [l/(m^2 h)]
$J^{s,exp}$	Steady state permeate flux: experimental data points [l/(m^2 h)]
J_0	Initial permeate flux [l/(m^2 h)]
k	Mass transfer coefficient [m/s]
k_c	Filtration coefficient [Unit of k depends on value of n]
k_1	Effective mass transfer coefficient [m/s]
L	Cake thickness [μm]
l	Length of the hollow fiber cartridge [cm]
M	No. of data points at each operating condition [dimensionless]
m	Compressibility of the cake layer [dimensionless]
MWCO	Molecular weight cut-off [kDa]
N	No. of steady state data points [dimensionless]
ΔP	Trans-membrane pressure drop [Pa]
PAN	Polyacrylonitrile
q and ε_{c0}	Pressure dependence parameters of cake porosity [dimensionless]
R_c	Cake layer resistance [m^{-1}]
Re	Reynolds number [dimensionless]
R_m	Membrane Hydraulic resistance [m^{-1}]
Sc	Schmidt number [dimensionless]
Sh	Sherwood number [dimensionless]
t	Time [s]
TDS	Total dissolved solids [mg/l]
TMP	Trans-membrane pressure [Pa]
UF	Ultrafiltration
y	Distance from central line of hollow fiber [μm]

Greek letters

α	Specific cake layer resistance [m/kg]
α_0	Pressure independent parameter of specific cake layer resistance [m/kg]
δ	Mass transfer boundary layer thickness [μm]
ε_c	Cake porosity [dimensionless]
ρ_c	Cake density [kg/m^3]
σ	Reflection coefficient [dimensionless]

them, oil present in water can be categorized into 3 groups depending on the droplet size. If the droplet size is > 150 μm, it is termed as free oil and is termed as emulsion, if droplet size is < 20 μm. Third category is dispersed oil having droplet size between 20 and 150 μm. Membrane technology is highly efficient compared to the conventional methods and its efficiency depends on the feed characteristics and membrane properties [9]. Most commonly used polymeric membranes are polysulfone, polyethersulfone, polyvinylidene fluoride, polyacrylonitrile (PAN) and cellulose acetate. Microfiltration (MF) and ultrafiltration (UF) membranes with molecular weight cut-off between 50 and 200 kDa have been employed widely for removal of oil and grease from effluent streams. Chakrabarty et al., studied filtration of synthetic oily water using different UF membranes of varying selectivity [5]. Karakulski et al., used tubular UF membrane modules of different materials for treatment of harbor and simulated emulsions and compared the efficiency of the treatment process [11]. Salahi et al., used five different types of membranes (two MF and three UF) for treatment of oily effluent from Tehran refinery and modeled the flux decline using Hermia's model and cake filtration was found to be the predominant mechanism of flux decline [8]. Daiminger et al., used membranes to separate oil from water by inducing coalescence [12]. Similar feed was treated by Rezaei et. al., using ceramic filtration modules and thus observed total organic carbon (TOC) removal efficiency of above 95% [7]. Ceramic MF membranes were also employed by Hua et al., for treatment of oily water and the effect of various parameters on separation efficiency was studied [10]. Matos et. al., carried out ultrafiltration of oily waste water and optimized the performance to find suitable parameters in total recycle mode [13]. Al-obeidani et. al., investigated effects of operating conditions on microfiltration of oily water using hollow fiber membranes [14]. However, all these works lack comprehensive modeling for prediction of profiles of permeate flux and oil concentration in permeate to quantify the system performance and subsequent scale up.

In the present work, real life effluent stream obtained from Railway Workshop, South Eastern Railway, Kharagpur, India, is treated to obtain clean water. The effluent was generated during washing of the railway coaches in their cleaning schedule. The major content of this effluent was oil, grease and dirt. Removal of contaminants was carried out in two stages. The effluent was pre-filtered through fine sand bed to remove dirt and suspended particles. The output of this stream was then treated by hollow fiber UF membrane to remove oil and grease. Effects of operating conditions on filtration performance were also investigated. The fouling mechanism of the membrane was identified. A model under the framework of cake controlling cross flow filtration was formulated to simulate the profiles of permeate flux and concentration of oil in permeate. Such work is envisaged to help in designing and up scaling hollow fiber based filtration systems for treatment of oily water from an industrial origin.

2. Theory

2.1. Identification of flux decline

Mechanism of flux decline can be identified by analyzing the time history of permeate flux in an unstirred dead end filtration process. Hermia et al. proposed an equation, given by Eq. (1), which represents the characteristic curves of a batch filtration process and is widely used by several researchers to identify the mode of flux decline [15,16].

$$\frac{d^2t}{dV^2} = k'\left(\frac{dt}{dV}\right)^n \tag{1}$$

where, V is the cumulative flux at any time point t and k' and n are system parameters. The value of n varies depending on the mode of filtration. Corresponding to the four types of flux decline mechanisms, following relations are derived from Eq. (1):

i. Complete pore blocking model ($n = 2$)

$$\ln\left(\frac{1}{J}\right) = \ln\left(\frac{1}{J_0}\right) + k_c t \tag{2a}$$

ii. Standard pore blocking model ($n = 1.5$)

$$\frac{1}{\sqrt{J}} = \frac{1}{\sqrt{J_0}} + k_c t \tag{2b}$$

iii. Intermediate pore blocking model ($n = 1$)

$$\frac{1}{J} = \frac{1}{J_0} + k_c t \tag{2c}$$

iv. Cake filtration model ($n = 0$)

$$\frac{1}{J^2} = \frac{1}{J_0^2} + k_c t \tag{2d}$$

In the above equation, J, is the permeate flux at any time point t, J_0 is the initial permeate flux and k_c is the filtration coefficient. Unit of k_c changes depending on the value of n.

2.2. Model development for cross flow filtration

As described in subsequent sections, cake filtration was identified as governing flux decline mechanism. The schematic of the filtration along with the co-ordinate system is presented in Fig. 1.

A differential element representing the control volume located at the edge of cake layer but entirely residing within mass transfer boundary is shown in Fig. 1 along with the descriptions of input output solute flux terms. A mass balance on solute (oil in this case) within this element results in following equation [17]:

$$\rho_c(1-\varepsilon_c)\frac{dL}{dt} = Jc - D\frac{dc}{dy} - Jc_p \tag{3a}$$

In the above equation ρ_c, ε_c and L are density, porosity and thickness of cake layer respectively, c is concentration of oil based on mass fraction, represented by TOC, D is its diffusivity and c_p is the permeate concentration. Eq. (3a) is a non-homogeneous ordinary differential equation valid within $0 \le y \le \delta$, where, δ is mass transfer boundary layer thickness. It satisfies the boundary condition,

$$\text{at } y = 0,\ c = c_0 \tag{3b}$$

where, c_0 is solute concentration of feed. Solution of Eq. (3a) using the boundary condition (Eq. (3b)) is

$$\frac{Jy}{D} = \ln\left(\frac{(c-c_p) - \left(\frac{\rho_c(1-\varepsilon_c)}{J}\frac{dL}{dt}\right)}{(c_0-c_p) - \left(\frac{\rho_c(1-\varepsilon_c)}{J}\frac{dL}{dt}\right)}\right) \tag{4}$$

Eq. (4) is evaluated at the interface of cake and mass transfer boundary layer, i.e., at $y = \delta$, $c = c_c$,

where, c_c is the constant solute concentration of cake layer and the resultant expression on rearrangement is

$$\rho_c(1-\varepsilon_c)\frac{dL}{dt} = J\frac{(c_c-c_p) - (c_0-c_p)e^{J/k}}{(1-e^{J/k})} \tag{5a}$$

where, k is the mass transfer coefficient $\left(=\frac{D}{\delta}\right)$. Initial condition of above equation is

$$\text{at } t = 0,\ L = 0 \tag{5b}$$

Solute transport through the membrane can be presented by modified Kedem-Katchalsky equation [18]

$$Jc_p = \underbrace{B(c_c - c_p)}_{\text{Diffusive flux}} + \underbrace{(1-\sigma)c_{avg}J}_{\text{Convective flux}} \tag{6}$$

where, B is solute permeability through the membrane, σ is the reflection coefficient and c_{avg} is the average solute concentration in the membrane phase defined as $c_{avg} = \frac{c_c - c_p}{\ln\left(\frac{c_c}{c_p}\right)}$.

In Eq. (6), first term on right hand side represents diffusive transport through the membrane phase and second term corresponds to the convective transport. Phenomenological equation for permeate flux can be written as,

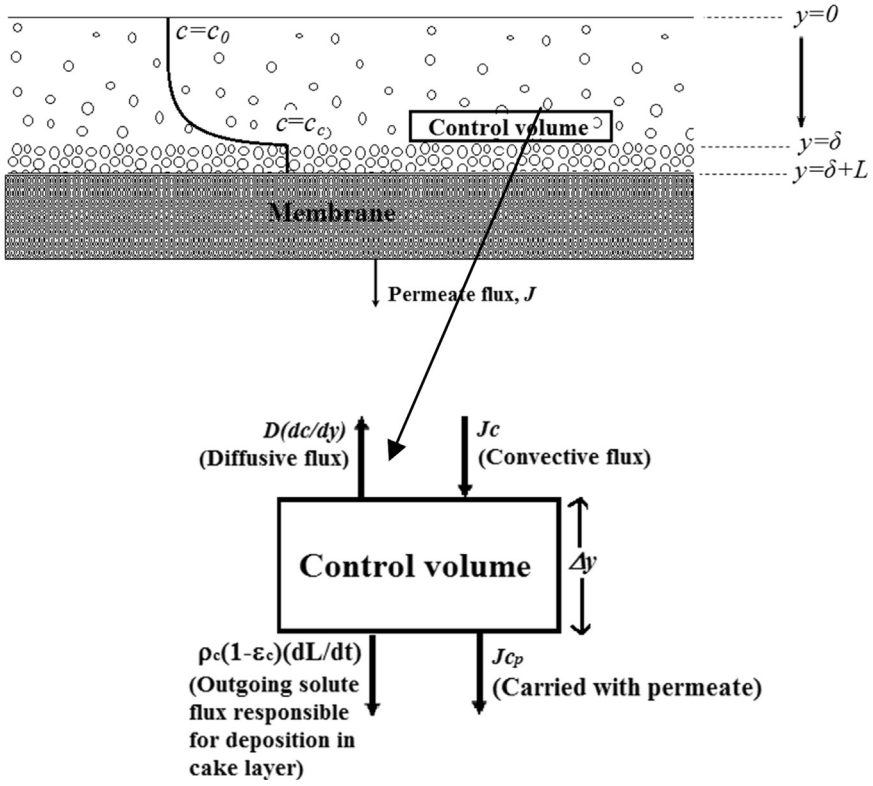

Fig. 1. Schematic diagram of membrane system and cake layer.

$$J = \frac{\Delta P}{\mu(R_m + R_c)} \tag{7}$$

where, ΔP is the transmembrane pressure, μ is the viscosity of the permeating solution, R_m is the membrane hydraulic resistance and R_c is the cake layer resistance. R_c can be expressed in terms of cake layer properties as,

$$R_c = \alpha(1 - \varepsilon_c)\rho_c L \tag{8}$$

where, α is specific cake layer resistance. Eqs. (5) to (8) present a set of differential-algebric equations and their simultaneous solution presents the evolution of permeate flux, permeate concentration and thickness of cake layer.

2.3. Estimation of model parameters

2.3.1. Evaluation of specific cake layer resistance(α)

From the flux characteristic equation (Eq. 2d), for unstirred batch experiment, the filtration constant, k_c is expressed as [19],

$$k_c = \frac{2c_0\alpha}{J_0 R_m} \tag{9}$$

The slopes obtained from $\frac{1}{J^2}$ verses t at different membrane pressures, are used to compute corresponding α values using Eq. (9). α is then related to transmembrane pressure drop as,

$$\alpha = \alpha_0(\Delta P)^m \tag{10}$$

where, m represents the compressibility of cake layer and α_0 is the pressure independent parameter.

2.3.2. Mass transfer coefficient (k)

Mass transfer coefficient, k depends on the velocity in the flow tube, solute and solution properties and geometry of flow channel. Sherwood number for flow through the hollow fiber is obtained from Leveque equation for laminar flow given as [20,21]:

$$Sh = 1.62\left(\mathrm{Re}\, Sc\frac{d}{l}\right)^{\frac{1}{3}} \tag{11}$$

where, d is the hollow fiber diameter, Re is Reynolds number in flow channel, Sc is the Schimdt number and l is the length of the fiber. It has been reported in literature that in most of the cases of cake filtration, mass transfer coefficient, k is a weak function of operating pressure (ΔP) to account for the porous nature of the wall of flow channel [22,23] and this dependency is expressed as,

$$k_1 = k(1 - a\exp(-b\Delta P)) \tag{12}$$

where, k_1 is the effective mass transfer coefficient, k is mass transfer coefficient described by Eq. (11), a and b are pressure dependence parameters.

2.3.3. Cake layer porosity (ε_c)

The solute particles being oil droplets, are not hard spheres but are malleable and the droplet size varies with pressure due to coalescence. Several researchers have reported coalescence of oil droplets under pressure and increase in droplet diameter during membrane filtration [5,24–26]. Due to the coalescence of oil droplets, the porosity of cake layer is not constant but varies with pressure affecting cake layer characteristics. Therefore, cake layer porosity varies with operating pressure and the dependency is proposed to as following:

$$\varepsilon_c = \varepsilon_{c0}(\Delta P)^q \tag{13}$$

where, ε_{c0} is porosity corresponding to incompressible cake and q is the exponent of dependency on ΔP. For incompressible cakes q is equal to 0 and cake porosity is also independent of pressure. Higher value of q indicates that cake porosity increases with TMP due to increased coalescence.

2.3.4. Oil diffusivity and cake layer density

Main constituent of the waste water obtained from railways includes mixture of paraffin oils and grease. The diffusivity of oils varies with the molecular weight of the constituent oils. Therefore, the average diffusivity for oil can be considered as a mean of diffusivity of lower hydrocarbons ($D \sim 4.35 \times 10^{-9}$ m^2/s) and slightly higher molecular weight paraffins ($D \sim 1.4 \times 10^{-10}$ m^2/s) [27]. Based on this, the average value of 8×10^{-9} m^2/s is taken as a representative diffusivity for the mixed group of oily substances present in the effluent stream. The cake layer consists of oil droplets densely packed and the density of this layer, ρ_c, is obtained from literature as 810 kg/m^{3}corresponding to hydrocarbons [28,29].

2.3.5. Estimation of model parameters

The model parameters need to be estimated are: cake layer concentration c_c; pressure dependence parameters for mass transfer coefficient a, b; solute transport coefficients in membrane phase, B and σ and porosity coefficients, ε_{g0} and q. Parameters c_c, a, b, B and σ can be estimated from the experimental data at steady state using the method outlined below. At steady state, the expression of permeate flux is derived from Eq. (5) as,

$$J^s = k_1 \ln\left(\frac{c_c - c_p^s}{c_0 - c_p^s}\right) \tag{14}$$

Similarly, solute transport through the membrane at steady state becomes,

$$J^s c_p^s = B(c_c - c_p^s) + (1 - \sigma)\left(\frac{c_c - c_p^s}{\ln\left(\frac{c_c}{c_p^s}\right)}\right)J^s \tag{15}$$

The coupled algebraic Eqs. (14) and (15) are solved simultaneously for all operating conditions and five parameters (c_c, a, b, B and σ) are optimized by minimizing the following sum,

$$S = \sum_{i=1}^{N}\left(\frac{J_i^{s,\,cal} - J_i^{s,\,\exp}}{J_i^{s,\,\exp}}\right)^2 + \sum_{i=1}^{N}\left(\frac{c_{pi}{}^{s,\,cal} - c_{pi}{}^{s,\,\exp}}{c_{pi}{}^{s,\,\exp}}\right)^2 \tag{16}$$

where, $J_i^{s,\,cal}$ and $c_{pi}{}^{s,\,cal}$ are calculated permeate flux and permeate concentration at steady state for i^{th} experimental condition. $J_i^{s,\,\exp}$ and $c_{pi}{}^{s,\,\exp}$ are corresponding experimental data. N is the total number of steady state data points, which is equal to 15 corresponding to exhaustive combination of three CFR and five TMP values.

ε_{g0} and q are pressure dependence parameters of cake porosity and these are determined from experimental transient flux at different operating conditions by minimizing the error function given by:

$$errf = \sum_{j=1}^{N}\sum_{i=1}^{M}\left(\frac{J_{i,j}^{cal} - J_{i,j}^{\exp}}{J_{i,j}^{\exp}}\right)^2 \tag{17}$$

where, $J_{i,j}^{\exp}$ are experimental flux values for j^{th} experiment i^{th} time point respectively and $J_{i,j}^{cal}$ is the corresponding calculated transient permeate flux. M represents the number of data points in each experiment, which is equal to 34 in this study.

3. Experiments

3.1. Materials

Hydrolyzed PAN co-polymer hollow fiber membrane module of molecular weight cut-off (MWCO) 70 kDa was purchased from M/s Technoquips Separation Pvt. Ltd., India. Oily waste water was obtained from Railway Wagon workshop, Kharagpur, India (22.3°N, 87.23°E).

3.2. Methods

3.2.1. Membrane characterization

3.2.1.1. Hydraulic permeability. The membrane was compacted with distilled water at 140 kPa pressure for 3 h. Membrane permeability was measured by plotting pure water flux at different TMP. The slope of the line gives the hydraulic permeability (L_p) of the membrane. It was $(7.4 \pm 0.37) \times 10^{-10}$ m/Pa s.

3.2.1.2. Field emission scanning electron microscope (FESEM) analysis. To observe the morphology of cross section of fibers, membranes were freeze fractured using liquid nitrogen and to observe the inner surface, membranes were cut into two halves laterally using sharp blade. Membrane cross section and inner surface were coated with platinum using sputtering machine and observed under FESEM (model: JSM 7610 make: JEOL, Japan).

3.2.1.3. Fourier transform infrared (FTIR) spectroscopy. The formation of cake layer on the membrane surface was analyzed using FTIR spectroscopy (model: Spectrum 100 supplied by Perkin Elmer, USA). Sample was cut into rectangular pieces of 60 mm × 20 mm dimension and air dried for overnight before measurement. Full scan was done in the range 650–4000 cm^{-1} in attenuated total reflectance (ATR) mode, which eliminates the need for sample preparation using potassium bromide pellets.

3.2.2. Experimental set-up and procedure

3.2.2.1. Sand bed filtration. The waste water was passed through fine sand bed of average grain size 840 µm, porosity 0.38, column diameter 0.05 m and column length 0.2 m, to remove dust, dirt and suspended solids. Treated water was then characterized as feed to UF.

3.2.2.2. Cross flow filtration. Output of the sand bed was used as feed to the cross-flow filtration set-up shown in Fig. 2. The feed was pumped to the hollow fiber using a booster pump and the retentate flow rate was monitored using a rotameter. The cross flow rate (CFR) and trans-membrane pressure (TMP) were set independently using bypass and the retentate valves. Experiments were conducted at 5 TMPs (21, 35, 48, 62 and 104 kPa) and 3 CFRs (14, 28 and 40 l/h) corresponding to Reynolds number 25, 50 and 70, respectively. Permeate was collected using a measuring cylinder at known time intervals and the flux was calculated. The permeate stream was analyzed in terms of pH, conductivity, total dissolved solids (TDS), total organic content (TOC) and turbidity. After each run, the membrane was washed by a cleaning cycle consisting of 15 min acid wash using 0.1 M hydrochloric acid solution and 15 min alkali wash using 0.2 N sodium hydroxide solution. After cleaning, the membrane was rinsed thoroughly by passing distilled water for 30 min to remove traces of contaminants. Effectiveness of cleaning was confirmed by measuring the hydraulic permeability of the membrane at the end of each cleaning cycle. It was found that the permeability value was within ± 5% of consecutive experiments. All experiments were conducted in triplets and the mean value of permeate flux and permeate concentration along with the error bars are reported in figures.

3.2.2.3. Dead end filtration set-up. Cross flow experimental set up as explained in previous section was operated as a dead end membrane filtration unit by closing the retentate valve completely. The operating pressure was varied by adjusting the bypass valve. Filtration experiments were carried out at varying pressure and permeate flux was measured. The batch mode flux data, thus obtained was used to identify the flux decline mechanism.

3.2.3. Feed and permeate characterization

3.2.3.1. TOC content. The oily contaminants present in the effluent stream consisted of a combination of organic components of different molecular weights. Therefore, the oil content in various streams was quantified as equivalent TOC using a TOC analyzer (model: TOC-L manufactured by: M/s Shimadzu) supplied by Swan Environmental Pvt. Ltd., India.

3.2.3.2. pH, TDS and conductivity. pH, TDS and conductivity of different streams were measured using a multi-parameter pocket tester (EUTECH Instruments Ltd. Singapore).

3.2.3.3. Particle size distribution. Particle size of feed was measured using Mastersizer (model: EPA2000). Particle size of filtrate was measured by Zetasizer (model: ZEN3600). Both the particle size analyzers were manufactured by M/s Malvern Instruments, UK.

3.2.3.4. Turbidity. Turbidity of various streams was measured by a digital turbidity meter (model: 331 make: Electronics India, India).

3.2.3.5. Flux recovery ratio (FRR). FRR value signifies the efficiency of cleaning process and is defined as

$$FRR = \frac{J_{wa}}{J_{wb}} \times 100\ \% \tag{18}$$

where, J_{wa} and J_{wb} are pure water flux after and before washing.

3.2.3.6. Flux decline ratio (FDR). FDR signifies the extent of fouling and is defined as

$$FDR = \frac{J_0 - J^s}{J_0} \times 100\ \% \tag{19}$$

where, J_0 and J^s represent the initial and final (steady state) permeate flux during an experiment. (Table 1).

4. Results and discussion

The feed stream obtained from Railways was highly contaminated with dirt and grease along with thick layer of oil floating on top. Fresh feed, as obtained, was characterized for pH and turbidity. The raw feed turbidity was measured to be 13.7 NTU. Sand bed filter was used to treat the raw feed which removed suspended particles effectively and the turbidity was reduced to 2.6 NTU. pH of the oily water remained unchanged at 6.5 before and after sand bed. The sand bed filter was operated under gravity and flow was adjusted at 80 l/day. Removal of suspended particles by the sand bed reduced load on UF membrane enhancing its life. Filtrate from sand bed was used as feed to membrane separation system. Properties of ultrafiltration hollow fiber membranes of hydrolyzed PAN co-polymer are tabulated as following:

Dead end filtration experiments were carried out as explained in Section 3.2.2 at three different operating pressures (21 kPa, 35 kPa and 48 kPa) and permeate flux was measured at various time intervals. The flux data thus obtained was used to calculate different functional forms

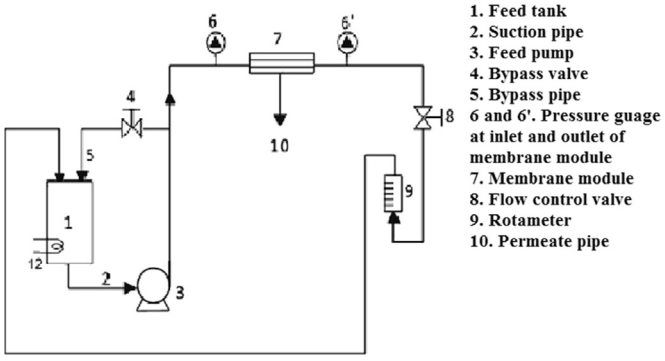

Fig. 2. Schematic diagram of experimental set-up for ultrafiltration.

Table 1
Properties of hollow fiber membrane.

Sl. No.	Property	Value
1.	Permeability (m/Pa s)	$7.4 \pm 0.37 \times 10^{-10}$
2.	MWCO (kDa)	70 ± 5
3.	Contact angle (°)[30]	82
4.	Internal diameter of fiber (μm)	640
5.	Average pore diameter (nm)	17
6.	Breaking stress (N/mm^2)[30]	1.5

of J according to Eq. (2) and goodness of fit was analyzed based on Hermia's model as explained in Section 2.1. The relations of J with t for different mechanisms are shown in Fig. 3. The graphical representation clearly indicates that cake filtration model fits the data best which is also supported by the correlation coefficients tabulated in Table 2.

The permeate flux as obtained from dead end filtration experiments was used to measure specific cake resistance parameters, α_o and m by measuring cake resistance (α) at various TMPs as explained in Section 2.3.1. α is calculated from the slope of Fig. 3(d) using Eq. (9) at each TMP, and $\ln(\alpha)$ is plotted against $\ln(\Delta P)$ to calculate α_o and m from intercept and slope, respectively (refer Fig. 4). The α_o and m are estimated as $(7.3 \pm 0.15) \times 10^{12}$ m/kg and 0.84 ± 0.02, respectively. Value of m indicates that the cake layer formed is compressible.

Filtration experiments were carried out in continuous cross flow mode as explained in Section 2.2 and permeate flux at various time points was noted under different operating conditions. The steady state values of the permeate flux were used to estimate the model parameters a, b, B, σ and c_c as explained in Section 2.3.5. The value of c_c was

Table 2
Correlation coefficient of fitting of Hermia's model.

Pressure (kPa) → / Model ↓	21	35	48
Complete pore blocking model	0.88	0.87	0.75
Standard pore blocking model	0.91	0.89	0.83
Intermediate pore blocking model	0.91	0.92	0.88
Cake filtration model	0.97	0.97	0.98

obtained as 62 ± 1 mg/l and the parameters a and b were 0.90 ± 0.02 and $(2 \pm 0.04) \times 10^{-5}$ Pa^{-1}, respectively. The parameters B and σ were obtained as $(4.8 \pm 0.04) \times 10^{-7}$ kg/(m^2 s) and 0.94 ± 0.02, respectively.

Using the estimated parameters, the steady state permeate flux at different TMP and CFR was computed and the comparison is presented in Fig. 5(a). The computed values agree remarkably well with the experimental data. From the variation, it is observed that steady state permeate flux increases with TMP at fixed CFR. The increase is linear up to 50 kPa and it is gradual thereafter. Variation clearly indicates the weak dependence of mass transfer coefficient with TMP and pressure independent flux is not attained in the studied range of TMP. However, effect of variation of cross flow rate is not significant.

Parameters calculated using steady state data are used to evaluate

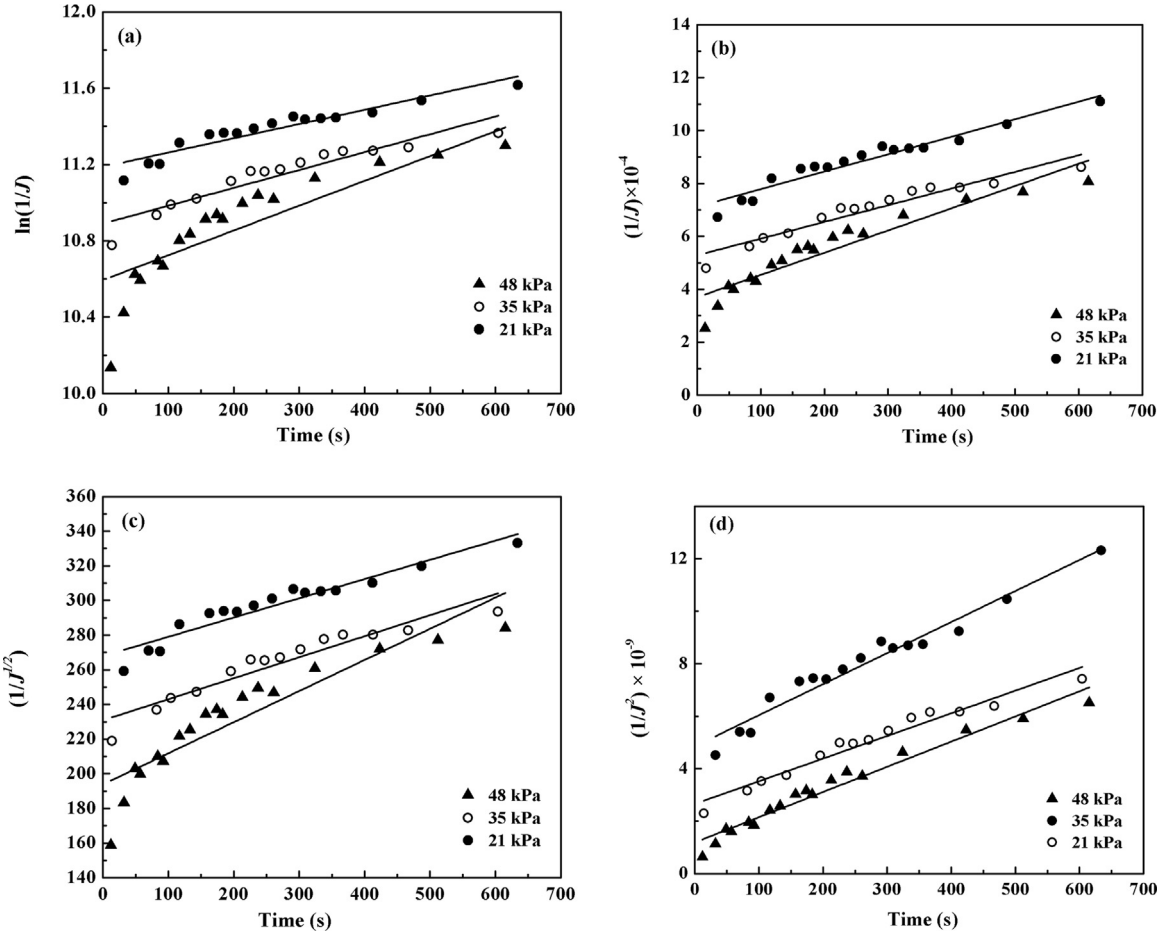

Fig. 3. Fitting of characteristic equation with batch cell flux data for (a) complete pore blocking model (b) intermediate pore blocking model (c) standard pore blocking model (d) cake filtration model. Error in measurement of J = ± 5%.

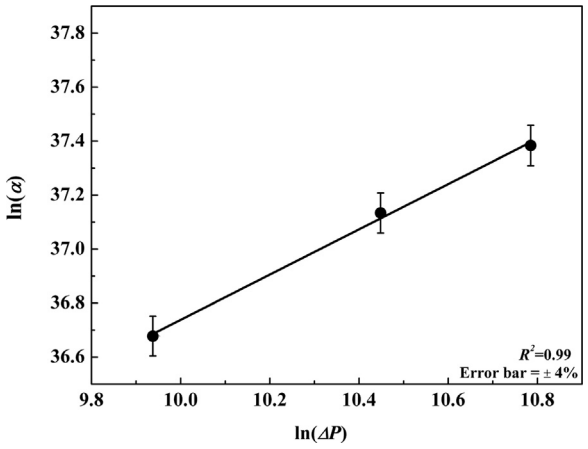

Fig. 4. Determination of specific cake resistance (α).

transient flux profile. Cake layer porosity is the only unknown parameter and its dependence on pressure is represented by Eq. (13). The values of ε_{c0} and q are obtained by minimizing the error function of Eq. (17). The optimization was carried out using standard Matlab optimizing algorithms. Values of ε_{c0} and q are obtained as 0.26 ± 0.01 and 0.1 ± 0.002, respectively. Using these values, the flux decline profiles are estimated and their comparison with experimental data is shown in Fig. 5(b) to (d). Corresponding profiles of cake layer thickness are also presented in these figures. Some typical trends can be observed. At any set of operating conditions, the cake layer thickness grows with time due to deposition of more solutes and correspondingly the permeate flux declines due to increase in cake layer resistance. However, growth of cake layer becomes sluggish in the long run of operation due to imposed forced convection of cross flow of retentate. An interesting observation can be made from Fig. 5(b) to (d). Rate of growth of cake layer thickness is rapid up to initial 10 min and it slows down thereafter, indicating quick build up of cake layer during initial period. The initial growth of the cake layer is due to the deposition of larger oil droplets resulting into a cake of very high porosity. Beyond 10 min, the smaller droplets continue to fill the interstitial voids thereby reducing the growth rate of the cake layer. For example, at 14 l/h CFR and 104 kPa TMP (Fig. 5(b)), cake layer thickness quickly becomes 0.68 μm at 10 min and then gradually increases to 2.26 μm at the end of 97 min. This trend has a direct consequence on permeate flux profile. At the same operating conditions, permeate flux declines rapidly within 10 min and slowly thereafter and eventually reaching to an almost steady state. Effect of TMP on cake layer thickness and permeate flux profile are apparent from these figures. More oil droplets are transported towards the membrane surface at higher TMP, thereby increasing thickness of cake layer. For example, at 14 l/h CFR, cake layer thickness increases from 1.5 to 2.25 μm as TMP is increased by almost five times, from 21 kPa to 104 kPa. However, pressure dependence of permeate flux is dictated by Eq. (7). Increase in pressure results in increase of driving force (numerator of Eq. (7)) as well as cake layer thickness and hence R_c (denominator of Eq. (7)). Between the interplay of these two factors, effect of driving force becomes dominant resulting in enhancement of permeate flux with TMP. For the same change of TMP (5 folds), steady state permeate flux increases from 5 to 18 l/m^2 h (3.6 times). Effects of CFR is not significant (in the range studied here) either on cake layer thickness or permeate flux profile. However, although small, there is slight reduction of cake layer thickness and marginal improvement of permeate flux with CFR, due to shearing

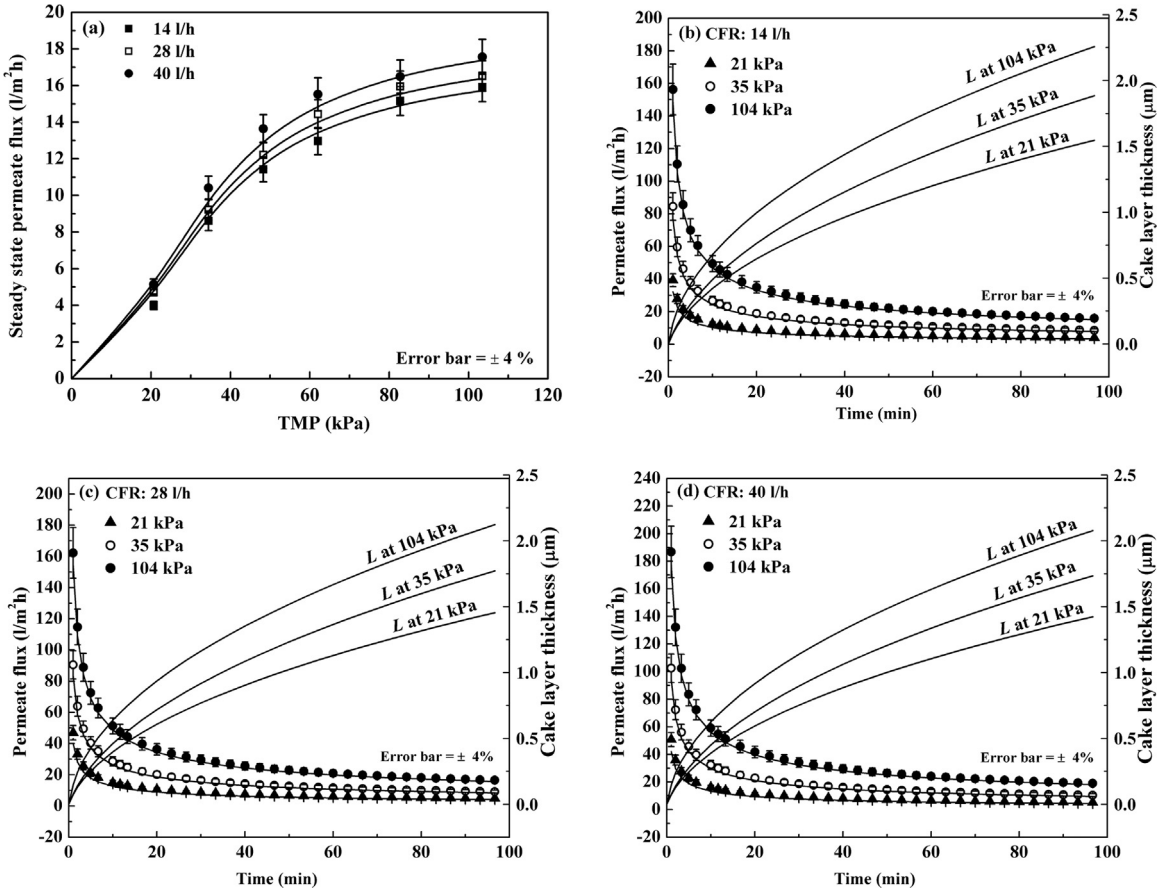

Fig. 5. Variation of (a) Steady state permeate flux with TMP. (b) to (d) Transient profiles of flux decline at various operating conditions. Scattered points represent experimental data points and continuous line represents modeled curve.

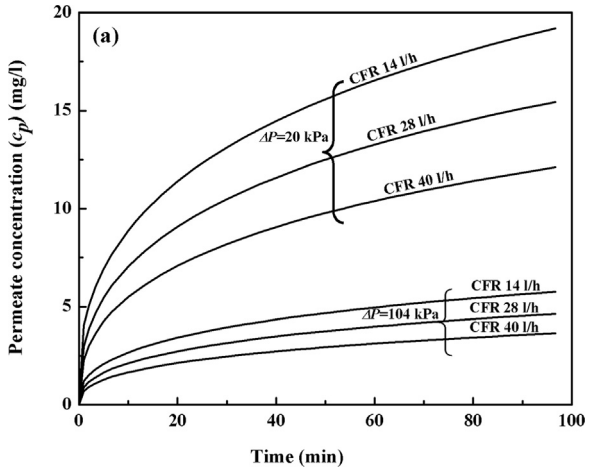

Fig. 6. Variation of permeate oil concentration with time.

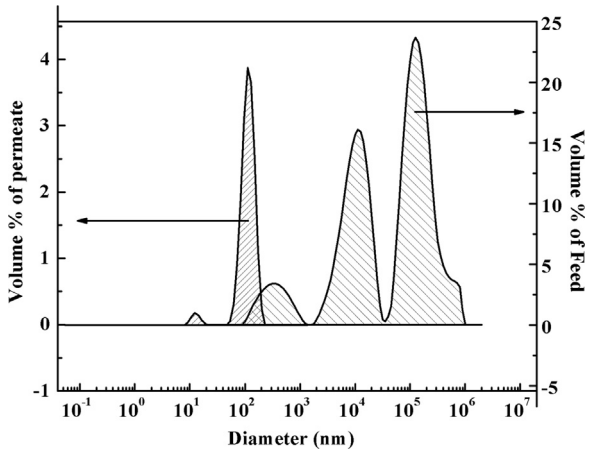

Fig. 7. Particle size distribution in feed and in permeate.

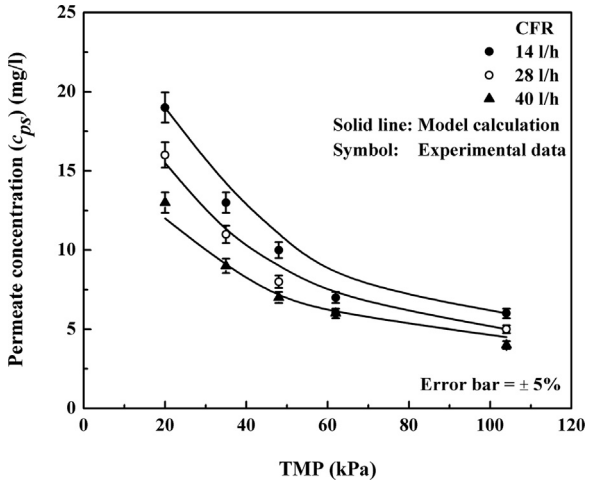

Fig. 8. Variation of permeate oil concentration with TMP at steady state.

action imparted by cross flow.

The model calculated profiles of oil concentration in permeate for various operating conditions are presented in Fig. 6. Three trends are evident from this figure. First, the oil concentration in permeate increases with time at fixed operating conditions. Second, effects of TMP and CFR are more dominant at lower TMP. Third, oil concentration in permeate is less at higher TMP. At fixed TMP and CFR, the cake layer grows in time resulting to transport of more oil droplets towards membrane surface. Although the membrane has pore diameter distribution (8–40 nm), average pore diameter of the membrane was 16 nm as observed from Figure A.1 in Appendix. A typical size distribution of oil droplets in feed and permeate (at 104 kPa and 40 l/h CFR) is shown in Fig. 7. Feed contains three distinct size fractions, 100–1000 nm, 2000–3 × 10^4 nm and 3 × 10^4 to 10^6 nm. The last fraction has the maximum population. In fact, there exists a negligible small fraction of oil having size range from 10 to 20 nm in the feed that was not visible in feed oil size distribution in the figure but it appeared distinctly in the permeate. Permeate has a small fraction of size range 10–20 nm and another major fraction of size 50–200 nm. As discussed earlier, more oil droplets are transported towards the membrane surface with progress of filtration time and smaller sized droplets (10–40 nm) are permeated through the membrane, thereby increasing the oil concentration in the permeate. However, as evident from Fig. 7, it is clear that some permeated oil droplets coalesce resulting to size as big as 200 nm. In fact, oil droplets being malleable, some larger sized droplets (than the membrane pore size) may be transported through the membrane.

At higher TMP, oil droplets coalesce to larger extent and bigger droplets are rejected by the membrane due to size exclusion thereby reducing its concentration. Enhanced degree of coalescence with TMP is also supported by the positive exponent in Eq. (13). For example, at 14 l/h CFR, after 60 min of filtration, oil concentration in filtrate is 16.5 mg/l at TMP 20 kPa whereas it is 5 mg/l at TMP 104 kPa. Effect of cross flow rate is more pronounced at lower TMP. Higher CFR results in enhanced forced convection along the length of the hollow fiber, preventing deposition of oil droplets by lowering the residence time and reducing the permeation of oil droplets through the membrane. Thus, oil concentration in permeate decreases with CFR. For example, at 20 kPa TMP, after 1 h, oil concentration in filtrate is reduced from 16.5 to 10.5 mg/l as CFR increases from 14 to 40 l/h. Variation of oil concentration at steady state with operating conditions is shown in Fig. 8. The trends corroborate with the transient profiles as already explained. Model predictions match remarkably well with the experimental data. From the graph, ultrafiltration process can be operated at 50 kPa TMP and 40 l/h with permeate concentration well below the permissible limit. Operating at higher pressure gives a marginal reduction in permeate concentration at the expense of higher operating cost.

Relative variation of diffusive and convective solute flux with operating conditions is presented in Fig. 9. Both Fig. 9(a) and (b) show that diffusive flux is almost five times the convective flux. As the bigger oil droplets form a blanket type cake layer on the membrane surface, effect of TMP on diffusive flux is marginal. However, convective flux increases with TMP almost twice as TMP increases from 21 to 35 kPa (Fig. 9(a)). Beyond 21 kPa, effect of TMP is marginal due to the presence of cake layer. Since oil concentration in cake layer (the upstream concentration across the membrane) remains constant, the diffusive flux is predominant over the convective flux. Effect of CFR (Fig. 9(b)) is insignificant on both diffusive and convective solute flux. Because of presence of cake layer over the membrane surface, CFR in hollow fiber does not influence the solute transport in membrane pores significantly.

To confirm the filtration mechanism as cake-formation, membrane cross section and inner surface morphology were analyzed using FESEM and results are shown in Fig. 10. Fig. 10(a) and (d) show the cross sectional view of fresh and fouled membrane. It is clear from full view of cross section that there exists porous microstructure sandwiched between dense skin layer on inner and outer surfaces of hollow fiber. The thickness of the inner skin layer, which is responsible for oil filtration, (Fig. 10(b) and (e)) shows that fouled membrane has higher skin thickness (16.9 μm) compared to fresh one (15.1 μm) indicating formation of cake layer. The cake layer thickness can be estimated by subtracting the average skin thicknesses of fresh membrane from fouled one, i.e. 1.8 μm. This data closely corroborates the modeled cake thickness value presented in Fig. 5(b). At higher resolution of inner wall of macrovoids of fouled membrane (Fig. 10(f)), deposit of solute

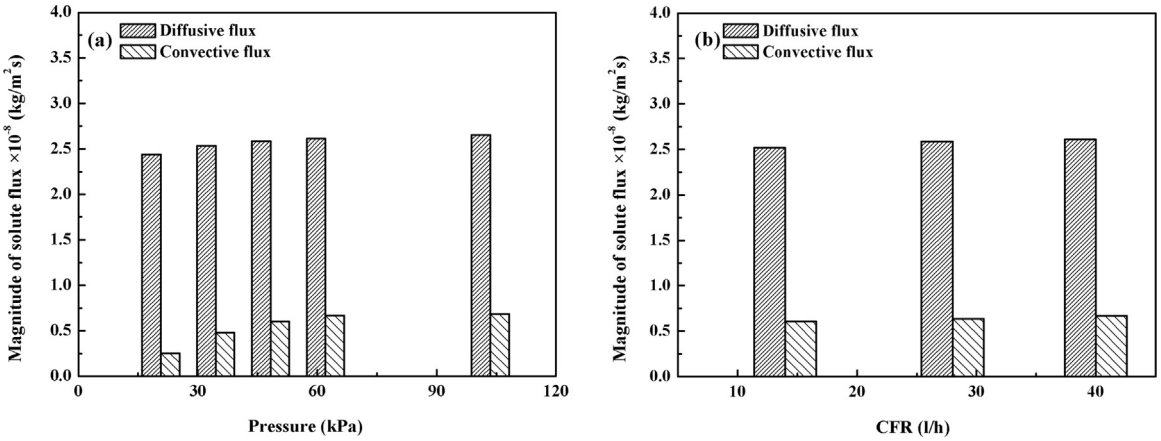

Fig. 9. Relative variation of diffusive and convective solute flux (a) with pressure, at 40 l/h CFR and (b) with CFR, at 62 kPa TMP.

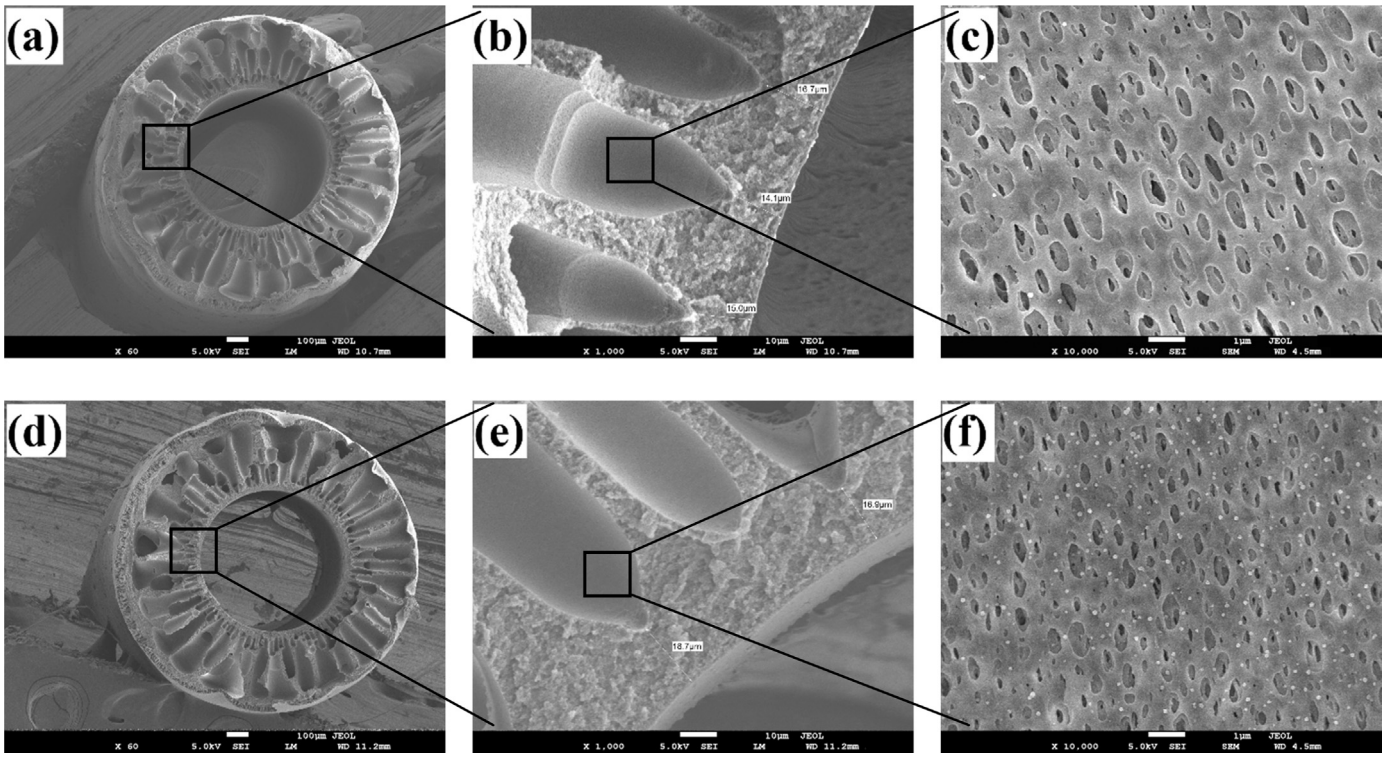

Fig. 10. FESEM micrographs of cross section of (a)-(c) fresh membrane; (d)-(f) fouled membrane.

particles can be observed, which is not present for fresh one (Fig. 10(c)). Formation of cake on the membrane surface can be clearly visualized in FESEM micrographs of inner surface of the membrane as shown in Fig. 11(a) to (d). A uniform deposition of solutes is observed on the entire inner surface of hollow fiber (compare Fig. 11(a) and (c)). The magnified image in Fig. 11(d) shows the presence of solute particles confirming the proposed cake-layer controlled mechanism of filtration. Feed consists of oil droplets from 10^2 to 10^6 nm, among which the larger droplets are directly rejected by the membrane. These droplets do not undergo coalescence due to high activation energy and small residence time. The smaller droplets having very low activation energy immediately undergo coalescence resulting into larger size droplets [31]. This, explains the formation of a thin cake layer of thickness ~ 1.8 μm even though the droplet size in feed consists of a significant fraction of oil droplets of diameter > 1 μm.

Nature of the cake layer on membrane surface is analyzed on fouled membrane surface with reference to a fresh membrane using FTIR spectrograph shown in Fig. 12. The transmittance peak at 2243 cm^{-1}, represents the cyanide (–CN) group of PAN molecules present on membrane surface [32,33]. Aliphatic groups are indicated by transmittance peaks at 2927 cm^{-1} and 2856 cm^{-1} representing the alkyl groups of oily material on membrane surface [33,34]. Existence of aromatic C=C bonds is confirmed by the peaks at 1749 cm^{-1} and 1457 cm^{-1} [33,35]. The aliphatic and aromatic organic compounds in the fouled membrane correspond to the paraffin oils present in the feed accumulated in the form of cake-layer.

The experimental values of FRR as obtained are plotted in Fig. 13(a) and observed to be varying between 75% and 90%. This indicates that after the filtration, the membrane can be regenerated with moderate loss of permeate flux after each cycle. The observed FDR values at various operating conditions, as shown in Fig. 13(b), vary between 73% and 90% indicating maximum loss of 90% of initial flux value during filtration. There is an increasing trend of FDR values with pressure, which may be attributed to the increase the cake layer thickness with pressure. However, with the acid-alkali treatment, the lost flux could be recovered which is reflected in higher values of FRR.

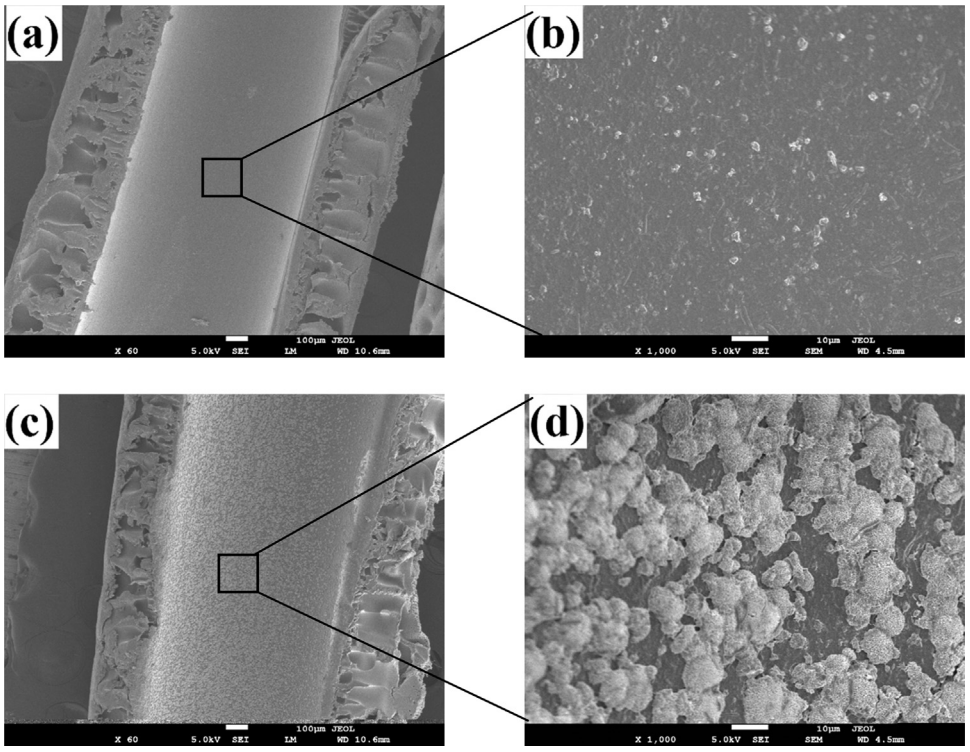

Fig. 11. FESEM micrographs of inner surface of (a) and (b) fresh membrane; (c) and (d) fouled membrane.

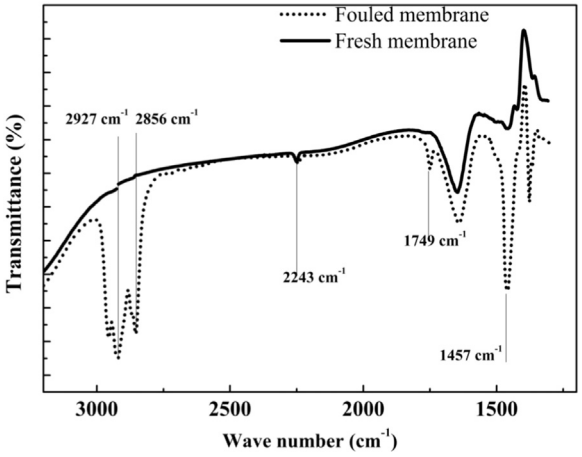

Fig. 12. FTIR Analysis of fresh and fouled membrane.

A thorough analysis of overall performance of UF reflects that concentration of oil in permeate is 3.75 mg/l at 104 kPa and 40 l/h CFR which is much below the permissible limit. The permeate quality in terms of TDS, pH, conductivity, turbidity and oil content are well within the admissible limit of industrial discharge water (Table 3).

5. Conclusion

Real life effluent from Railway workshop was treated to remove oil using hollow fiber based cross flow ultrafiltration. UF unit could remove oil effectively by reducing its concentration from 45 mg/l to 3.75 mg/l. The turbidity was reduced from 13.6 NTU to 1.02 NTU. Cake filtration was found to be the prevailing mechanism during cross flow ultrafiltration. A physical model from first principles was proposed and successfully implemented to quantify the transient transport of solvent and oil through the membrane. It was established that coalescence of oil droplets under pressure during filtration added to the filtration resistance aiding in oil selectivity. Solute transport through the membrane was found to be diffusion dominated. Cross flow in hollow fiber did not affect the solute transport through the membrane significantly

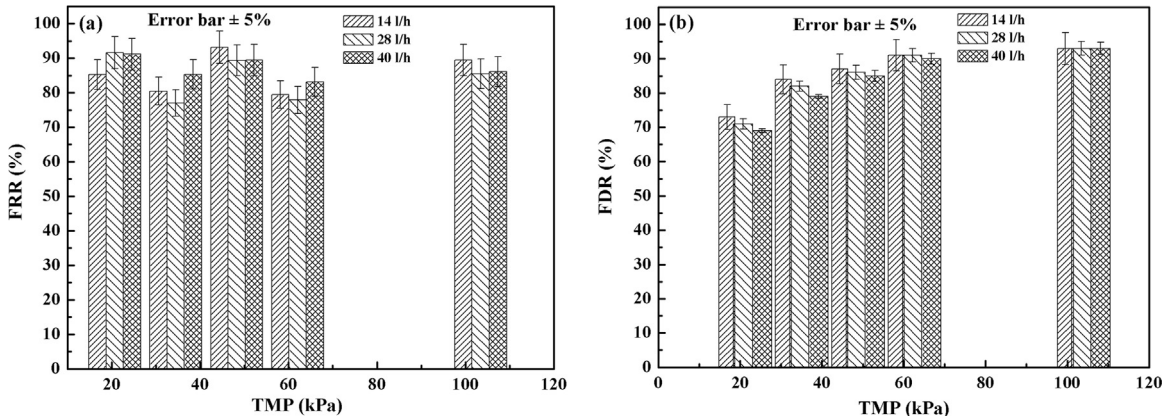

Fig. 13. (a) Variation of FRR and (b) FDR with TMP.

Table 3
Characteristics of various streams at 104 kPa and 40 l/h.

Sl. No.	Property	After sand bed	After UF at 104 kPa pressure and 40 l/h flow rate	Permissible limit in India
1	pH	7.2	6.46	5.5–9
2	Conductivity (μS/cm)	137.4	5.5	1500
3	TDS (mg/l)	98.1	86.9	500
4	Average particle size (μm)	113	0.35	NA
5	Turbidity (NTU)	2.6	1.02	10
6	Oil (mg/l)	45.41	3.75	10

due to presence of cake layer. FESEM and FTIR analysis confirmed the formation of cake layer. Membrane was regenerated by more than 90% using acid alkali treatment. The developed model and determination of various critical cake characteristic parameters can be used for design and scale-up of industrial oil effluent treatment systems.

Acknowledgement

This work is partially supported by a grant from the SRIC, IIT Kharagpur under the scheme no. IIT/SRIC/CHE/SMU/2014-15/40, dated 17-04-2014.

Appendix A. Supplementary material

Supplementary data associated with this article can be found in the online version at http://dx.doi.org/10.1016/j.memsci.2018.01.051.

References

[1] M. Cheryan, N. Rajagopalan, Membrane processing of oily streams, Wastewater Treat. Waste Reduct. 151 (1998).
[2] P. Kajitvichyanukul, Y.-T. Hung, L.K. Wang, Membrane technologies for oil–water separation, in: L.K. Wang, J.P. Chen, Y.-T. Hung, N.K. Shammas (Eds.), Membrane and Desalination Technologies, Humana Press, Totowa, NJ, 2011, pp. 639–668, , http://dx.doi.org/10.1007/978-1-59745-278-6_15.
[3] J.W. Patterson, Ind. Wastewater Treat. Technol. (1985).
[4] M. Gryta, K. Karakulski, A.W. Morawski, Purification of oily wastewater by hybrid UF/MD, Water Res. 35 (2001) 3665–3669, http://dx.doi.org/10.1016/S0043-1354(01)00083-5.
[5] B. Chakrabarty, A.K. Ghoshal, M.K. Purkait, Ultrafiltration of stable oil-in-water emulsion by polysulfone membrane, J. Membr. Sci. 325 (2008) 427–437, http://dx.doi.org/10.1016/j.memsci.2008.08.007.
[6] T.Ã. Rajaram, A. Das, Water pollution by industrial effluents in India : Discharge scenarios and case for participatory ecosystem specific local regulation, Futures 40 (2008) 56–69, http://dx.doi.org/10.1016/j.futures.2007.06.002.
[7] S. Rezaei, H. Abadi, M. Reza, M. Hemati, F. Rekabdar, T. Mohammadi, Ceramic membrane performance in micro filtration of oily wastewater, Desalination 265 (2011) 222–228, http://dx.doi.org/10.1016/j.desal.2010.07.055.
[8] A. Salahi, A. Gheshlaghi, T. Mohammadi, S. Siavash, Experimental performance evaluation of polymeric membranes for treatment of an industrial oily wastewater, Desalination 262 (2010) 235–242, http://dx.doi.org/10.1016/j.desal.2010.06.021.
[9] M. Padaki, R.S. Murali, M.S. Abdullah, N. Misdan, A. Moslehyani, M.A. Kassim, N. Hilal, A.F. Ismail, Membrane technology enhancement in oil – water separation, A Rev. 357 (2015) 197–207.
[10] F.L. Hua, Y.F. Tsang, Y.J. Wang, S.Y. Chan, H. Chua, S.N. Sin, Performance study of ceramic microfiltration membrane for oily wastewater treatment, Chem. Eng. J. 128 (2007) 169–175, http://dx.doi.org/10.1016/j.cej.2006.10.017.
[11] K. Karakulski, A. Kozlowski, A.W. Morawski, Purification of oily wastewater by ultrafiltration, Sep. Technol. 5 (1995) 197–205.
[12] U. Daiminger, W. Nitsch, P. Plucinski, S. Hoffmann, Novel techniques for oil / water separation, J. Membr. Sci. 99 (1995) 197–203.
[13] M. Matos, A. Lobo, E. Fernández, J.M. Benito, C. Pazos, J. Coca, Recycling of oily ultrafiltration permeates to reformulate O / W emulsions, Colloids Surf. A: Physicochem. Eng. Asp. 331 (2008) 8–15, http://dx.doi.org/10.1016/j.colsurfa.2008.06.004.
[14] S.K.S. Al-Obeidani, H. Al-Hinai, M.F.A. Goosen, S. Sablani, Y. Taniguchi, H. Okamura, Chemical cleaning of oil contaminated polyethylene hollow fiber microfiltration membranes, J. Membr. Sci. 307 (2008) 299–308, http://dx.doi.org/10.1016/j.memsci.2007.09.048.
[15] J. Hermia, Constant pressure blocking filtration laws-application to power law non-Newtonian fluids, Trans. IChmE 60 (1982) 183–187.
[16] C. Ho, A.L. Zydney, A combined pore blockage and cake filtration model for protein fouling during microfiltration, J. Colloid Interface Sci. 399 (2000) 389–399, http://dx.doi.org/10.1006/jcis.2000.7231.
[17] V.M. Starov, A model and mathematical representation for membrane concentration and purification of macromolecular solutions containing low molecular weight contaminants, J. Membr. Sci. 79 (1993) 241–251, http://dx.doi.org/10.1016/0376-7388(93)85119-H.
[18] B.M. Bungay, H.K. Lonsdale, M.N. de Pinho, Synthetic membranes: science, Eng. Appl. (1986).
[19] A. Kunz, V. Reginatto, N. Durán, Combined treatment of textile effluent using the sequence Phanerochaete chrysosporium–ozone, Chemosphere 44 (2001) 281–287.
[20] G.B. Van der Berg, I.G. Rácz, C.A. Smolders, Mass transfer coefficients ultrafiltration in cross-flow, J. Membr. Sci. 47 (1989) 25–51, http://dx.doi.org/10.1016/S0376-7388(00)80858-3.
[21] V. Gekas, B. Hallström, Mass transfer in the membrane concentration polarization layer under turbulent cross flow: I. Critical literature review and adaptation of existing sherwood correlations to membrane operations, J. Memb. Sci. 30 (1987) 153–170.
[22] S. Mondal, A. Cassano, F. Tasselli, S. De, A generalized model for clarification of fruit juice during ultrafiltration under total recycle and batch mode, J. Memb. Sci. 366 (2011) 295–303, http://dx.doi.org/10.1016/j.memsci.2010.10.015.
[23] S.T. Johnston, W.M. Deen, Hindered convection of ficoll and proteins in agarose gels, Ind. Eng. Chem. Res. 41 (2002) 340–346, http://dx.doi.org/10.1021/ie010085s.
[24] M. Hlavacek, Break-up of oil-in-water emulsions induced by permeation through a microfiltration membrane, J. Membr. Sci. 102 (1995) 1–7.
[25] P. Srijaroonrat, E. Julien, Y. Aurelle, Unstable secondary oil / water emulsion treatment using ultrafilltration: fouling control by backflushing, J. Membr. Sci. 159 (1999) 11–20.
[26] J. Floury, A. Desrumaux, J. Lardieres, Effect of high-pressure homogenization on droplet size distributions and rheological properties of model oil-in-water emulsions, Innov. Food Sci. Emerg. Technol. 1 (2000) 127–134.
[27] F.P. Lees, P. Sarram, Diffusion coefficient of water in some organic liquids, J. Chem. Eng. Data 16 (1971) 41–44.
[28] D.S. McIntyre, G.B. Stirk, A method for determination of apparent density of soil aggregates, Aust. J. Agric. Res. 5 (1954) 291–296, http://dx.doi.org/10.1071/AR9540291.
[29] J. Jarsj, G. Destouni, B. Y, Retention and volatilisation of kerosene: Laboratory experiments on glacial and post-glacial soils, J. Contam. Hydrol. 17 (1994) 167–185.
[30] R. Mukherjee, S. De, Adsorptive removal of nitrate from aqueous solution by polyacrylonitrile – alumina nanoparticle mixed, J. Membr. Sci. 466 (2015) 281–292, http://dx.doi.org/10.1016/j.memsci.2014.05.004.
[31] Y. Miyagawa, K. Katsuki, R. Matsuno, S. Adachi, Effect of oil droplet size on activation energy for coalescence of oil droplets in an O/W emulsion, Biosci. Biotechnol. Biochem. 79 (2015) 1695–1697, http://dx.doi.org/10.1080/09168451.2015.1039482.
[32] A.T. Krummel, M.T. Zanni, Evidence for coupling between nitrile groups using DNA templates: a promising new method for monitoring structures with infrared spectroscopy, J. Phys. Chem. B 112 (2008) 1336–1338, http://dx.doi.org/10.1021/jp711558a.
[33] J. Coates, R.A.M. Ed, J. Coates, Interpretation of infrared spectra, a practical approach, 2000, pp. 10815–10837.
[34] H.S. Mansur, C.M. Sadahira, A.N. Souza, A.A.P. Mansur, FTIR spectroscopy characterization of poly (vinyl alcohol) hydrogel with different hydrolysis degree and chemically crosslinked with glutaraldehyde, Mater. Sci. Eng. C 28 (2008) 539–548, http://dx.doi.org/10.1016/j.msec.2007.10.088.
[35] G.I. Andrade, E.F. Barbosa-Stancioli, A.A.P. Mansur, W.L. Vasconcelos, H.S. Mansur, Small-angle X-ray scattering and FTIR characterization of nanostructured poly (vinyl alcohol)/silicate hybrids for immunoassay applications, J. Mater. Sci. 43 (2008) 450–463, http://dx.doi.org/10.1007/s10853-007-1953-7.